Chemical Science

ROYAL SOCIETY OF CHEMISTRY

EDGE ARTICLE

View Article Online
View Journal | View Issue

Cite this: *Chem. Sci.*, 2021, **12**, 6159

All publication charges for this article have been paid for by the Royal Society of Chemistry

Excited state character of Cibalackrot-type compounds interpreted in terms of Hückel-aromaticity: a rationale for singlet fission chromophore design†

Weixuan Zeng, [a] Ouissam El Bakouri, [b] Dariusz W. Szczepanik, *[cd] Hugo Bronstein *[ae] and Henrik Ottosson *[b]

The exact energies of the lowest singlet and triplet excited states in organic chromophores are crucial to their performance in optoelectronic devices. The possibility of utilizing singlet fission to enhance the performance of photovoltaic devices has resulted in a wide demand for tuneable, stable organic chromophores with wide S_1–T_1 energy gaps (>1 eV). Cibalackrot-type compounds were recently considered to have favorably positioned excited state energies for singlet fission, and they were found to have a degree of aromaticity in the lowest triplet excited state (T_1). This work reports on a revised and deepened theoretical analysis taking into account the excited state Hückel-aromatic (instead of Baird-aromatic) as well as diradical characters, with the aim to design new organic chromophores based on this scaffold in a rational way starting from qualitative theory. We demonstrate that the substituent strategy can effectively adjust the spin distribution on the chromophore and thereby manipulate the excited state energy levels. Additionally, the improved understanding of the aromatic characters enables us to demonstrate a feasible design strategy to vary the excited state energy levels by tuning the number and nature of Hückel-aromatic units in the excited state. Finally, our study elucidates the complications and pitfalls of the excited state aromaticity and antiaromaticity concepts, highlighting that quantitative results from quantum chemical calculations of various aromaticity indices must be linked with qualitative theoretical analysis of the character of the excited states.

Received 20th January 2021
Accepted 24th March 2021

DOI: 10.1039/d1sc00382h

rsc.li/chemical-science

Introduction

Singlet exciton fission in organic molecules has the potential to significantly improve the efficiency of silicon-based photovoltaics through the reduction of thermalization losses. By absorbing a single higher energy photon, bringing a molecule to a singlet excited state, and converting this state into two equivalent lower energy triplet excited states one can potentially increase the single-junction photovoltaic limit up to 35%.[1,2] In order to achieve this, strict energetic conditions must be met; the lowest triplet (T_1) energy levels must be >1.11 eV (the bandgap of silicon) and the singlet energy level must be $\sim 2 \times T_1$ (so that singlet fission can occur). The development of design rules that allow for the identification and synthesis of new singlet fission chromophores is therefore arguably one of the most important challenges in functional organic materials research today. There have been several proposed design rules including the use of diradicaloid systems,[3–5] the assessment of the diradicaloid character of a chromophore,[6,7] and the manipulation of aromaticity to engineer the excited states,[8–12] which has led to a diverse range of structures in the hunt for improved singlet fission materials.[13–15] However, the fact that linear acenes remain the most successful chromophore for use in singlet fission photovoltaics, despite their well-documented instability,[16,17] demonstrates that more work must be done to understand the underlying design principles.

Our ambition is to develop refined design rules based on aromaticity as this can facilitate the identification of novel ways for the tailoring of molecules that function as chromophores for singlet fission photovoltaics. Aromaticity comes in different forms, *e.g.*, Hückel-,[18] Möbius-,[19,20] Baird-,[17–29] and spherical

[a]*Department of Chemistry, University of Cambridge, Cambridge, CB2 1EW, UK. E-mail: hab60@cam.ac.uk*

[b]*Department of Chemistry – Ångström Laboratory, Uppsala University, 751 20 Uppsala, Sweden. E-mail: henrik.ottosson@kemi.uu.se*

[c]*Department of Theoretical Chemistry, Faculty of Chemistry, Jagiellonian University, Gronostajowa, 2, 30-387 Kraków, Poland. E-mail: dariusz.szczepanik@uj.edu.pl*

[d]*Institut de Quìmica Computacional i Catàlisi, Departament de Química, Universitat de Girona, C/ Maria Aurèlia Capmany, 69, 17003 Girona, Catalonia, Spain*

[e]*Cavendish Laboratory, University of Cambridge, Cambridge, CB3 0HE, UK*

† Electronic supplementary information (ESI) available: Plots of NICS-*XY* scans, AICD, $EDDB_H$, spin density distribution and structural data. List of compounds include the following: the parent **CIBA**, substituted Cibalackrots, structurally altered Cibalackrot compounds and further modifications of the **CIBA** scaffold. See DOI: 10.1039/d1sc00382h

aromaticity.[30,31] Of relevance for the study presented herein are Hückel-aromaticity of closed-shell cycles with $4n + 2\pi$-electrons and Baird-aromaticity of cycles with $4n\pi$-electrons in their triplet $\pi\pi^*$ states.[22,25,32,33] According to quantum chemical calculations the Baird-aromaticity concept can also be extended to the lowest singlet excited state of simple annulenes,[34–36] supported by spectroscopic observations.[27,32,37,38] Lately, the concepts have been utilized to rationalize a range of photophysical and photochemical properties and processes.

Cibalackrot-type compounds (indolonaphthyridines), some of which can be proved to undergo singlet fission, were recently considered by one of us to have a degree of aromaticity in the lowest triplet excited state (T_1).[9] The basis for the conclusions was the observation of negative nucleus independent chemical shifts (NICS) in the pyrrole rings, which were interpreted as indicative of some influence of 4π-electron pyrrole dicationic rings. Based on this finding it was suggested that these compounds were Baird-type aromatics. The remarkable photostability of the Cibalackrot chromophore, alongside its facile tuneability, also makes it an attractive candidate for use in singlet fission photovoltaics. Another recent example of a singlet fission material which, based on computations, was suggested to have Baird-aromatic character in its triplet state is dipyrrolonaphthyridinedione (**DPND**).[10] In this context, it can be noted that compounds with $4n\pi$-electron cycles have been reported to show high photostability both in excited triplet and singlet states,[32,39] a feature that could be traced to excited state Baird-aromatic character.[19]

Yet, even though the predominant form of aromaticity in the first $\pi\pi^*$ excited states is the Baird-type aromaticity of $4n\pi$-electron cycles there are caveats. For example, a $\pi\pi^*$ triplet state can be of Hückel–Baird hybrid type as earlier found for a quinoid compound (**TMTQ**) in its T_1 state.[40,41] The T_1 state of such a compound has a central unit simultaneously influenced by both Hückel-aromaticity and Baird-aromaticity. Also, electronically excited states can be described by pure Hückel-type aromaticity, as observed for the charge-transfer state of a 6-aminosubstituted fulvene-based molecular motor where a 6π-electron cyclopentadienyl anionic ring makes an important contribution.[42] With this background it is obvious that the excited state aromaticity concept has its complications and pitfalls, and it should be important to outline these as precisely as possible so as to enable a more efficient design of molecules with targeted properties. Thus, we would here like to report on a deepened and broadened analysis of the aromatic character of Cibalackrot-type compounds in their T_1 states. Are Cibalackrot-type compounds Hückel-aromatic in their T_1 states?

We argue that with a proper description of the excited state aromatic character of Cibalackrot-type compounds we can, in a second part of this study, go further and make use of qualitative arguments to design new chromophores based on this scaffold. We outline the basic scope and limitations of this chromophore as well as various derivatives in the context of its application in singlet fission materials. In addition, the exploration could serve as a guide on how to interpret and apply the concepts of excited state aromaticity and antiaromaticity, avoiding the pitfalls that undoubtedly exist. A more comprehensive and proper view on how various forms of aromaticity and antiaromaticity impact on the excited state energies of molecules should enable a more rational and efficient development of optically active compounds for, *e.g.*, singlet fission photovoltaics.

Results and discussion

Focusing on the Cibalackrot-type compounds, we first dissected the effects of aromaticity in both the ground state (S_0) and the T_1 state of the parent Cibalackrot molecule (**CIBA**). An improved understanding of the role of aromaticity in its S_0 and T_1 states is core to an improved strategy for further design of singlet fission chromophore candidates based on this molecule. Then, with such an understanding, routes on how to select substituents and how to further alter the Cibalackrot core (*e.g.*, by benzannelation) so as to manipulate the excited state energy levels for singlet fission are presented. Finally, we reveal how the knowledge gained can be utilized to tune the excitation energies of **DPND** derivatives. The analysis is based on computed aromaticity indices, including nucleus independent chemical shifts scans (NICS-*XY*) and NICS values at 1.7 Å ($NICS(1.7)_{zz}$),[43,44] plots of the anisotropy of the induced current density (AICD),[45] the geometric harmonic oscillator model of aromaticity (HOMA),[46] and the electronic aromatic fluctuation (FLU)[47] and multicentre (MCI) indices.[48]

Parent Cibalackrot

In the description of **CIBA** we label the various rings as shown in Fig. 1. Fused rings are labelled with two letters so that, *e.g.*, AB and CC′ represent the perimeters of the indole-like 9-membered ring and the central 10-membered ring, respectively. For the identification of Cibalackrot-type compounds with suitable features for singlet fission it is crucial to understand the aromaticity effects in both the S_0 and the T_1 states as the T_1 energy ($E(T_1)$) can be linked to the difference in the total counts of aromatic cycles in the two states.

In the ground state (S_0), the two benzene rings (A/A′) with six π-electrons should have marked Hückel-aromatic character (Fig. 1). This is supported by all aromaticity indices; the magnetic indices, *i.e.*, the π-electron-only AICD plots and the NICS-*XY* scans reveal diamagnetic ring currents and negative NICS values reaching −5.8 ppm (Fig. 2), the geometric HOMA index is 0.924, and the electronic FLU and MCI indices (0.003 and 0.053, respectively) all reveal aromatic character. In contrast, rings B and B′ display markedly positive NICS values, suggesting antiaromatic character, but the AICD plot does not reveal paratropic ring currents. Also, the HOMA value of rings B and B′ (0.269) corresponds to a nonaromatic situation. The two indole-units (AB and A′B′) of **CIBA** in S_0 have some moderate aromatic character according to HOMA (0.629) but not so according to NICS-*XY* and AICD.

According to Fig. 2, the CC′ moiety of **CIBA** in its S_0 state should resemble 1,5-dihydro-1,5-naphthyridine-2,6-dione (**NARID**, Fig. S1 and S2†). In S_0, **NARID** has NICS values reaching down to −4.4 ppm while the CC′ moiety in **CIBA** has NICS

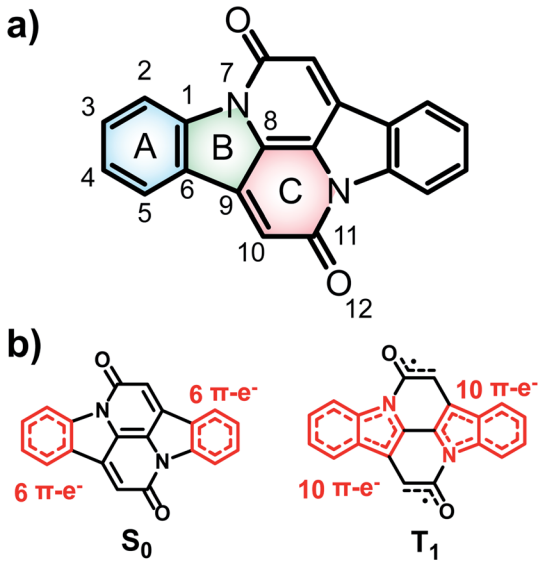

Fig. 1 Chemical structure of indolonaphthyridine-6,13-dione (**CIBA**), the relevant atoms and rings in symmetric positions are signed with an apostrophe. Hückel-aromatic units are marked as red in the lower panel: two benzene units in the S_0 state and two indole units in the T_1 state.

values at approximately −2 ppm, indicating nonaromatic character. This is corroborated by the AICD plot which does not display any significant ring current. The FLU values of the two compounds are similar (0.033 in **NARID** and 0.038 in the CC′ moiety of **CIBA**), although the HOMA differ because the CC′ unit in **CIBA** has a HOMA of 0.104 while it is 0.410 in **NARID**. Still, the CC′ moiety of **CIBA** in its S_0 state is best described as nonaromatic (Table 1).

When going to the T_1 state of **CIBA** the aromatic character shifts between the rings when compared to the S_0 state. According to both NICS-*XY* and AICD the diamagnetic ring currents now expand from the 6π-electron A/A′ rings to the 10π-electron indole-like AB/A′B′ units. The changes in the HOMA values of various cycles also indicate interesting trends. First, the HOMA of the AB and A′B′ units in T_1 is high (0.754) revealing an enhanced aromatic character when compared to S_0. The HOMA values of the strongly aromatic A/A′ benzene rings decrease minutely while the HOMA of the pyrrole rings increases substantially. The electronic indices also reveal an increased aromatic character of the AB/A′B′ units as the FLU value in the T_1 state is lowered when compared to S_0. Also, the MCI value of the pyrrole rings is raised (0.011) while that of the two benzene rings is reduced modestly. Yet, is this aromatic character in the T_1 state of Baird-type or of Hückel-type but with a different extension (localization) than in the S_0 state?

To explore the type of aromaticity of the AB unit in the T_1 state of **CIBA** we analysed the ratios $\Delta FLU_{\alpha\beta}/FLU$ between the difference in spin-separated FLU values ($\Delta FLU_{\alpha\beta} = FLU_{\alpha} - FLU_{\beta}$) and the FLU. As noted above, the FLU value of the AB/A′B′ units in the T_1 state is lower than in the S_0 state (0.007 *vs.* 0.013, respectively), indicating an increase in the aromatic character. Now, the value of $\Delta FLU_{\alpha\beta}/FLU$ clarifies whether a cycle is Baird-

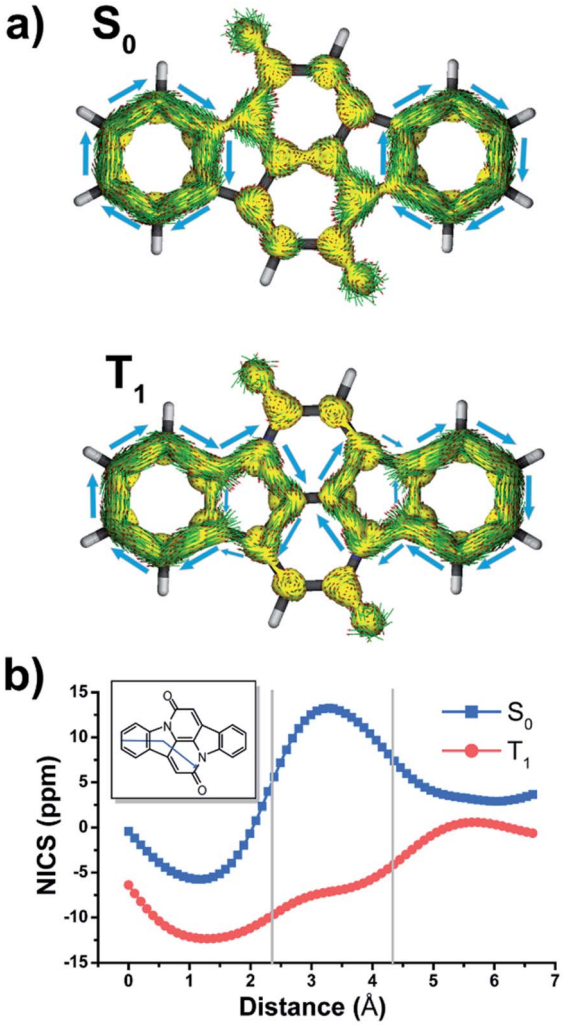

Fig. 2 (a) π-Electron ring currents according to AICD and (b) π-NICS-*XY* scan in the S_0 and T_1 states of **CIBA** calculated at GIAO/(U)B3LYP/6-311+G(d,p)//(U)B3LYP/6-311+G(d,p) level.

aromatic or Hückel-aromatic because $\Delta FLU_{\alpha\beta}$ is zero or negligible for a Hückel-aromatic cycle while it has a nonzero value for a Baird-aromatic cycle.[40,41] As references, indole and pyrrole in their closed-shell Hückel-aromatic S_0 states have $\Delta FLU_{\alpha\beta}/FLU$ values which are exactly zero while the Baird-aromatic indole and pyrrole dications in their triplet states have calculated values of 2.34 and 4.02, respectively (Table S1†). We now find that the $\Delta FLU_{\alpha\beta}/FLU$ ratios of the AB/A′B′ moieties and the B/B′ rings of T_1 state **CIBA** are low (−0.180 and −0.186, respectively), supporting an interpretation of the T_1 state in terms of Hückel-aromaticity. Furthermore, the cumulated atomic charges, obtained from a natural population analysis, in the AB/A′B′ and B/B′ rings are −0.418 and −0.400*e*, respectively. Finally, the aromatic character of the indole-like AB moiety is very similar to those of the separate (Hückel-aromatic) indole molecule in S_0 (Fig. S3a and b†). Combined this makes it clear that the indole units of **CIBA** in its T_1 state are predominantly Hückel-aromatic and not Baird-aromatic.

Table 1 Values of key aromatic indices for relevant cycles in **CIBA**

	S_0					T_1				
	A	B	C	AB	CC′	A	B	C	AB	CC′
π-NICS(1.7)$_{zz}$	−5.8	13.2	3.3	—	—	−12.3	−7.0	0.5	—	—
FLU	0.003	0.026	0.032	0.013	0.038	0.005	0.016	0.033	0.007	0.033
$\Delta FLU_{\alpha\beta}$/FLU	—	—	—	—	—	0.307	−0.180	−0.820	−0.181	−0.881
MCI	0.053	0.007	0.009	—	—	0.048	0.011	0.005	—	—
HOMA	0.924	0.269	0.146	0.629	0.104	0.898	0.493	0.225	0.754	0.072

The central **NARID** segment (CC′) of **CIBA** in its T_1 state clearly has a nonaromatic character according to both NICS and AICD, as well as to HOMA (0.072). The spin density reveals that the triplet diradical character is mainly localized within the **NARID** unit. As shown in Fig. 3, 69% of the spin density is localized on the CC′ segment, of which 22% and 40% at the two carbonyl O atoms and the two C_α atoms, respectively. Also, the spin density distribution within the central moiety is almost identical with that of **NARID** (Fig. S2c†). This observation on the triplet diradical localization to the CC′ moiety is consistent with the description of the T_1 state shown in Fig. 1. Moreover, the FLU value is rather high (0.033) indicating a nonaromatic situation. Although large $\Delta FLU_{\alpha\beta}$/FLU values are found for the CC′ segment in triplet state **CIBA** and **NARID** ($\Delta FLU_{\alpha\beta}$/FLU = −0.820 and −0.881, respectively), these values are due to the high spin density localized in this unit, and not to a Hückel–Baird hybrid character.

The interpretation of the altered Hückel-aromatic character when going from S_0 to T_1, and not a gain of Baird-aromaticity, is further corroborated by the analysis of global delocalization effects (involving heavy atoms only) using the electron density of delocalized bonds ($EDDB_H$) method (Fig. 3b).[49,50] The total electron delocalization in **CIBA** is slightly more effective in T_1 than in the S_0 state (+0.244*e*), but this is clearly an effect of enhanced π-conjugation (not cyclic π-delocalization) by unpaired electrons exclusively within the **NARID** moiety including the oxygen atoms (+1.408*e*), which to a large degree is compensated by the overall reduction of paired-electron delocalization (−1.164*e*) with respect to S_0. Thus, the lack of cyclic delocalization of spin-density and the actual reduction of paired-electron delocalization confirm that there is no Baird-type aromatic stabilization in **CIBA** in the T_1 state, at least not within the indole units. Here it is noteworthy **DPND** singlet fission chromophore was recently analysed,[51] and also for this compound there is a lack of triplet state Baird-aromatic character (see below and the ESI†), contrary to what was originally stated.[10]

Importantly, the S_1 state of **CIBA** is similar to the T_1 state since both states are described by single HOMO to LUMO excitations and they exhibit similar delocalization and hole–electron characters (Fig. S6 and Table S2†) along a tuning variable (Fig. 4a). With this information we postulate that one can tune the $E(T_1)$ and $E(S_1)$ in similar manners. The importance of this finding should be stressed as combined evaluations of the substituent effects only functions for species in which the T_1 and S_1 states are described by the same electron configuration. The opposite is illustrated by 5,10-bis(styryl) dibenzo[*a*,*e*]pentalene. This compound functions as a singlet fission chromophore,[52] in contrast to the parent compound, dibenzo[*a*,*e*]pentalene, which stems from a relative stabilization of the T_1 state as compared to the S_1 state upon the 5,10-bis(-styryl) substitution of dibenzo[*a*,*e*]pentalene (Fig. S8†) caused by a difference in the character of the T_1 and S_1 states.[8]

The results above show the spin density distribution and how the aromatic character is localized among the rings in the

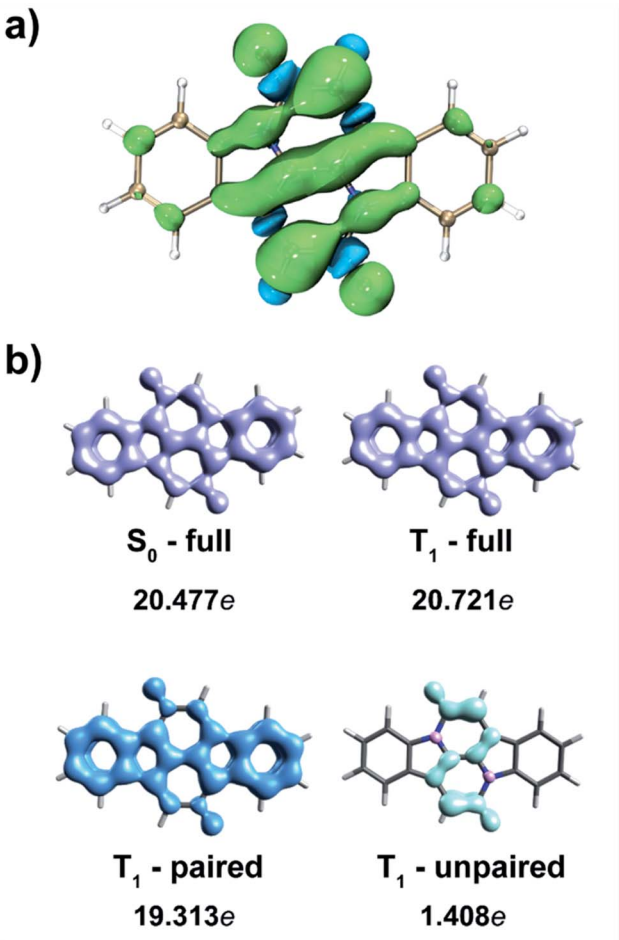

Fig. 3 (a) Spin density distribution in the T_1 state of **CIBA** ($\rho = 0.0008$), and (b) $EDDB_H$ isosurfaces ($\rho = 0.006$) with the corresponding electron populations in the S_0 state and in the T_1 state (total and dissected into paired and unpaired-electron components), calculated at (U) B3LYP/6-311+G(d,p) level.

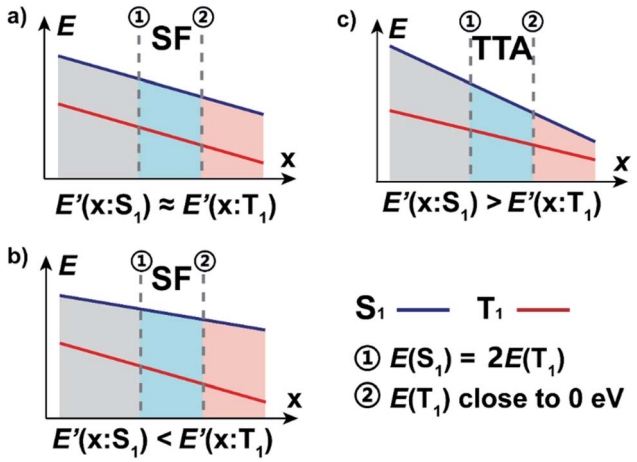

Fig. 4 Schematic of curves of energy levels (E) *vs.* variable indexes, the E' defined as the slope of E along the parameter x. There are three expected situations (a–c) each separated into three regions: (i) where aromaticity is not strong enough to ensure the stability (gray), (ii) balance regions with combination of proper energy levels and good stability (blue), and (iii) where the energy of T_1 is so low that it tends to undergo severe energy loss *via* the internal conversion process (red).

S_0, T_1 and S_1 states. The excited state aromatic characters of **CIBA** are closely linked to the Hückel aromatic contribution of the indole-like AB ring while the diradical character is focused to the central CC′ ring (supporting local resonance effects between C–C and C–O bonds according to the $EDDB_H$ results). Based on this, in the second part of the study we probe how to tune the excited state energy levels by substituents, by further benzannelation, and other modifications of the Cibalackrot scaffold. The knowledge gained from the three aspects can be combined into a design approach.

Substituted Cibalackrot-type compounds

The $E(T_1)$ of the parent **CIBA** is 1.73 eV for vertical excitation and 1.37 eV for adiabatic excitation, and as the spin density to a significant extent is localized to the two C_α atoms it should be possible to further delocalize the radical-pair character onto the substituents through proper choice of substituents. Such enhanced spin delocalizations should lower the T_1 state in energy. As the S_1 state, similar as the T_1 state, is described by the singly excited HOMO to LUMO excited configuration (Table S2†), the energy of the S_1 state ($E(S_1)$), could according to hypothesis above, change in energy to a similar extent as $E(T_1)$ when changing the substituents at the two C_α positions. If this holds then it should be possible to deduce a diagram with the excited state energies as functions of the spin density at the substituents as the variable by which the tuning is driven, similar as done earlier by two of us through usage of the (excited state) (anti)aromaticity as a tuning variable.[8] We tested this through the placement of radical stabilizing groups at the C_α-positions. The position of the threshold where $2E(T_1) = E(S_1)$ is located will depend on the $\Delta E(S_1 - T_1)$ and the slopes of the trendlines for $E(T_1)$ and $E(S_1)$.

The differently substituted Cibalackrots (**SCIBA**'s) in Fig. 5, as well as further ones in Fig. S9,† were analysed. The thiophene substituted model (**SCIBA1**) was taken from our previous work,[9] as it undergoes singlet fission. The benzene substituted model (**SCIBA2**) was also involved as it was reported to not undergo singlet fission.[53] Our computations now reveal that **SCIBA2** exhibits higher $E(T_1)$ and $E(S_1)$ compared to **SCIBA1** which makes the $E(S_1)/E(T_1)$ ratio smaller indicating a less efficient singlet fission process. By considering the dihedral angles between the substituents and the C_α–C(=O) bonds in the two compounds in the S_0 state (32.4° for **SCIBA1** and 45.8° for **SCIBA2**) it is clear that the conjugation to the phenyl groups in **SCIBA2** is weaker than to the thiopheno groups in **SCIBA1**, and this likely contributes to a lower $E(S_1)/E(T_1)$ ratio for **SCIBA2**. It is also possible that the different dihedral angles could influence the stacking of the compounds in the solid state, which can have effects on the formation of the key intermediate state of the singlet fission.[54,55] Thus, **SCIBA1** and **SCIBA2** provide a connection between the theoretical results herein and experimental data on functioning singlet fission chromophores.

We also tested cyano and vinyl substituents at the C_α atom as well as a range of different substituents with ethenyl or ethynyl moieties as spacers, including radical-stabilizing cyano, nitro, cyclooctatetraenyl (COTyl), cyclobutadienyl (CBDyl), borolyl, 2-2*H*-pyrazinyl, and bulky silyl groups (**SCIBA3–13**, **23–30**, Fig. S9†). Additionally, some of the above **SCIBA** compounds were further substituted with cyano groups on the 3/3′ positions of the parent **CIBA** core (**SCIBA15–22**), representing the effects of different substitution strategies. These species are discussed in the ESI.† Here it should be noted that **SCIBA23–30**, despite being synthetically unfeasible, enable us to examine the design model towards and until the extreme point corresponding to the full radical pair localization at the substituents **X**.

In the **SCIBA**s, the spin density at the C_α atoms of the parent Cibalackrot is delocalized onto the substituents and a gradually smaller portion of the spin density is located at the central CC′ moiety (Fig. S10†). Importantly, **SCIBA13** with two CBDyl substituents, despite being experimentally unrealistic, allow us to explore computationally the extreme point with the T_1 state completely described as a radical pair with the unpaired spin density at the two CBDyl groups (for the function of the CBDyl groups in this regard see the ESI†).

To evaluate the potential of the new substituted Cibalackrots to undergo singlet fission, the $E(T_1)$ and $E(S_1)$ were calculated and plotted against the spin population of the substituents **X** based on the optimized ground state geometry and the relaxed T_1 geometry of the compound, respectively (Fig. 6a and b). Linear fits with reasonable correlations were found and the higher the spin population on the substituents **X**, the lower $E(T_1)$ and $E(S_1)$ of the compound in question. This result agrees well with the radical delocalization approach for stabilization of the T_1 states. It is also apparent that the S_1 state displays a similar trend as the T_1 state. Notably, none of the ratios with vertical $E(T_1)$'s exceed 2, while all those with adiabatic $E(T_1)$'s do. Also, the spin population on the substituent **X**s are higher in the adiabatic T_1 geometries compared to those of the vertical geometries, which indicates that delocalization of

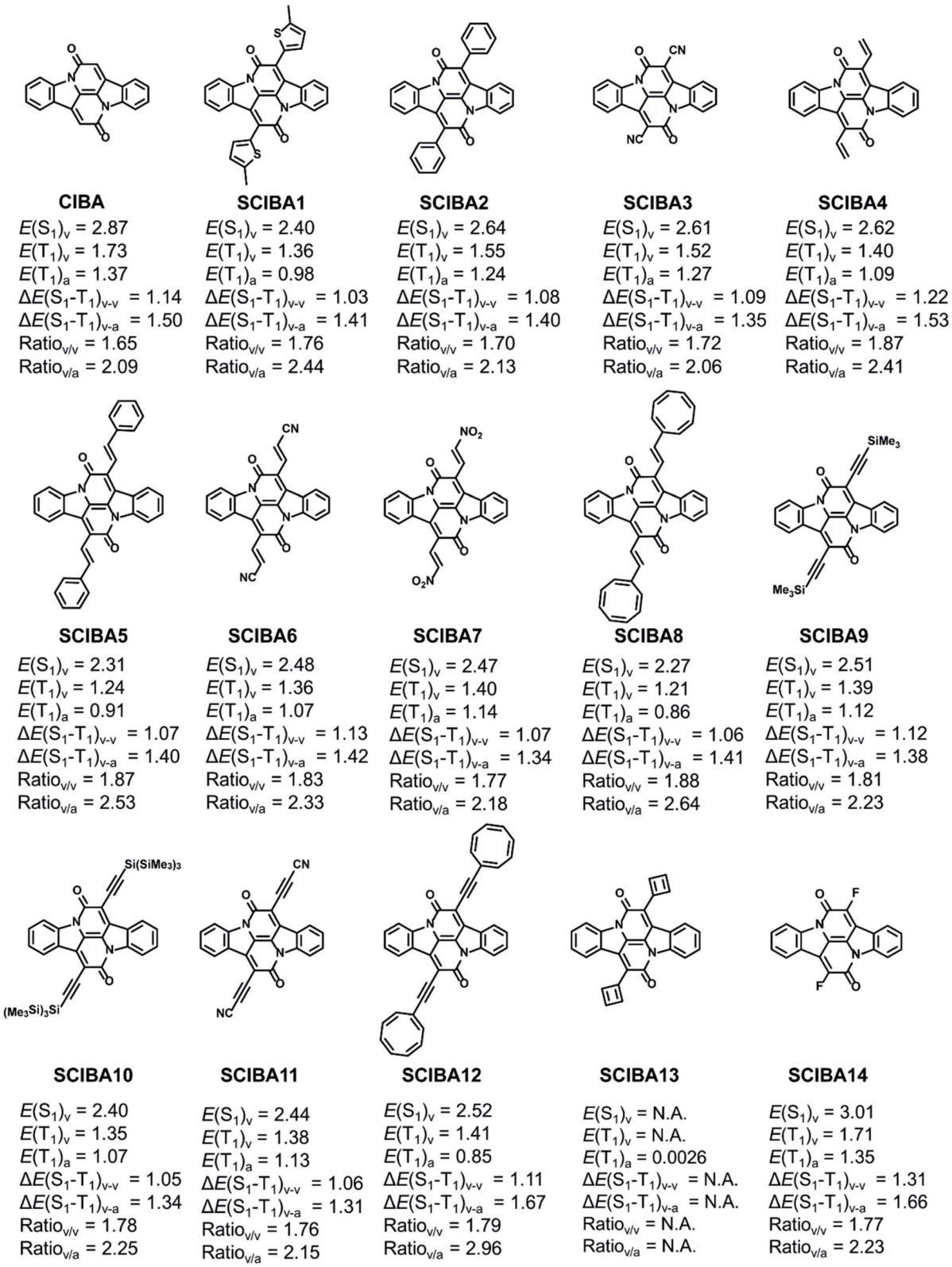

Fig. 5 Chemical structures and relevant excitation energies (in eV) of the parent **CIBA** and **SCIBA**'s. Calculations at TD-M06-2x/def2-SVP//M06-2X/def2-SVP level.

spin density onto the substituents **X** is accompanied by relaxation in the T_1 state. For **SCIBA1**, the Cibalackrot derivative which represents a functioning singlet fission chromophore,[9] the ratios are 1.76 and 2.44, respectively. Also notice, **SCIBA2** exhibits smaller spin population on the **X**s in both vertical and adiabatic excitation, compared to **SCIBA1**, which could be

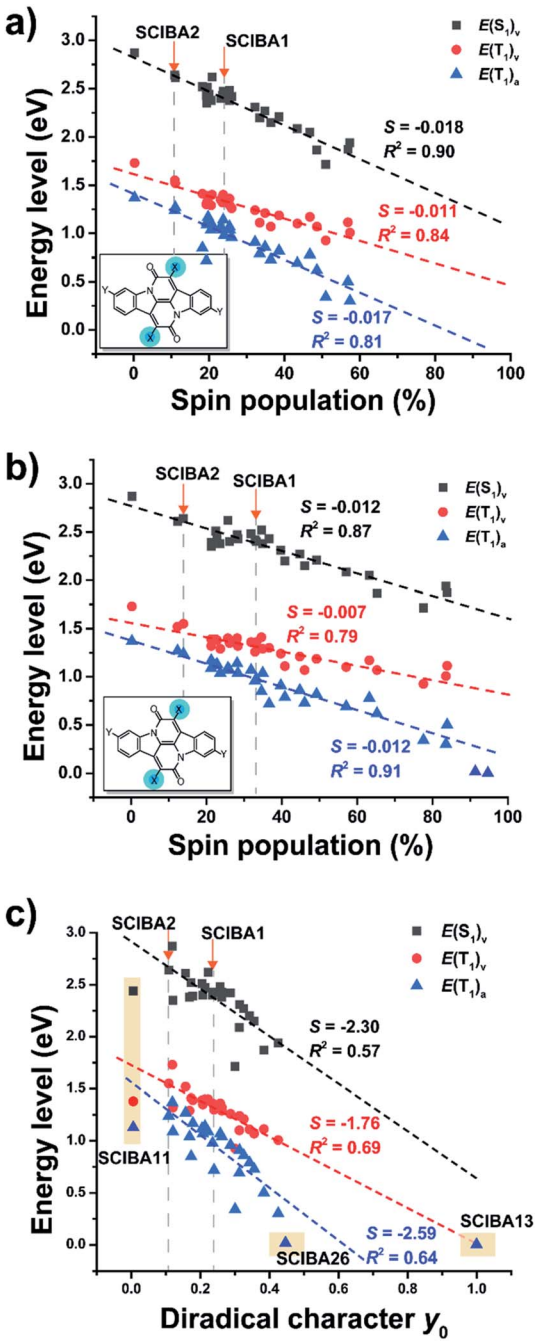

Fig. 6 Plots of excited state energies *versus* (a) the spin population on the substituent **X** moieties based on vertical excitation, (b) on the adiabatic excitation of T_1 geometries and (c) diradical character y_0 of parent **CIBA** and **SCIBA**s. Subscripted 'v' refers to vertical excitation energies based on S_0 geometries and 'a' refers to adiabatic excitation based on optimized T_1 geometries.

attributed to the different substituents and result in different singlet fission features.

Thus, with **SCIBA1** as an anchor we can conclude that several of the **SCIBA**'s likely will function for singlet fission, these being **SCIBA5**, **SCIBA8** and **SCIBA12**. Additional dicyano substitution at the 3/3′ positions, as in **SCIBA15–22**, could enhance their performance further as the $E(S_1)$ and $E(T_1)$ slightly decreased. Thus, the trend of the $E(S_1)$ and $E(T_1)$ indicates that fine-tuning *via* choice of substituents is a design strategy that provides an opportunity for tailoring chromophores to function in a singlet fission process. In the ESI† is also shown plots of $E(T_1)$ and $E(S_1)$ *versus* the spin populations at the C_α and at the CC′ moieties, respectively.

As predicted above **SCIBA13** represents the extreme case with essentially all unpaired spin density localized at the substituents, confirmed through the spin density distribution and the $EDDB_H$ analysis (Fig. S11 and S12†). The optimized open-shell singlet state of **SCIBA13** is located minutely below the optimized T_1 state, affording an $E(T_1)$ of 0.003 eV. Importantly, the $E(T_1)$ value of **SCIBA13** falls on the trendline extrapolated from the **SCIBA**'s with regular substituents, revealing that the design strategy functions all the way to this extreme point. Noteworthy, we refrained from calculations of the vertical excitation levels of S_1 and T_1 of **SCIBA13** due to the difficulty of the computational approaches for the calculation of excitations of compounds with open-shell ground states.

Here it can be noted that only a limited number of substituent groups **X** were found to allow for spin populations in the range 70–90%, *i.e.*, groups that allow for a predominant yet not complete localization of the two unpaired electrons onto the substituents **X** as for **SCIBA13**. After an extensive search three substituents with such features were identified, these being the 2-borolylvinyl, 3-borolylvinyl, and 2-2*H*-pyrazinylethynyl groups (for all compounds examined see **SCIBA23–30**, Fig. S13 and S14†). As noted above, most of these are not realistic, yet show that the trend sustains.

One can also ask if there are substituents that raise $E(T_1)$ and $E(S_1)$ relative to the parent **CIBA**? Such groups should be those that resist delocalization of spin density onto them. Through computations we find that fluoro substitution at C_α (**SCIBA14**) significantly raise $E(S_1)$ while $E(T_1)$ remains at a similar energy when compared to the parent **CIBA**. This could be assigned to the very strong electron withdrawing ability of the fluorine among the halogens, which resulted in the highest delocalization of the unpaired electrons at the carbonyl O and the C_α atoms (see ESI† for detailed discussion).

The diradical character in the S_0 state (y_0) has earlier been demonstrated to be an effective indicator in the search of novel candidates with potentials as singlet fission chromophores.[6,7] To explore the feasibility of the diradical character-based design of the Cibalackrots, we plotted the relevant excited state energies against the y_0 values in S_0 state (Fig. 6c). The correlation with the linear fit is now slightly weaker than the plots based on the spin population in the T_1 state. Yet, considering that the diradical character y_0 is a property calculated in the S_0 state while the spin population is taken at the optimal T_1 state geometry, the poorer correlation can be understood. Moreover, the y_0 value provides a quicker prediction of the state energies of a novel compound than the spin density in the T_1 state. Unsurprisingly, the y_0 value correlates best with the vertical $E(T_1)$. Notably, we excluded two compounds from the fit of $E(T_1)$ and $E(S_1)$ against y_0, **SCIBA11** and **SCIBA13**. For further discussion see the ESI (Fig. S18†).

We can now apply our earlier developed geometrical model where the $E(S_1)$ and $E(T_1)$ are plotted against a variable along which the energies vary.[8] In the diagram that results the singlet fission chromophores are located towards the right side. Previously we calculated the degree of (anti)aromaticity in S_0 or T_1 as the variable against which $E(T_1)$ and $E(S_1)$ are plotted, yet now we use the unpaired spin density at **X** or C_α (Fig. S19†) or the diradical character value y_0. However, this principle requires that the T_1 and S_1 states are (i) described similarly, *i.e.*, by the same electron configuration except for the multiplicity difference, and (ii) that the exchange interaction is constant throughout the set of molecules explored. The latter requires that HOMO and LUMO are similarly distributed in the various compounds.

Benzannelated Cibalackrot-type compounds

Having demonstrated the effect of the extent of localisation of spin density in the T_1 state to the C_α atoms on the T_1 energy levels we now turn to the peripheral aromatic rings (AB/A′B′ rings) of the Cibalackrot scaffold. Since our results above suggest that the formation of the Hückel-type excited state aromatic pyrrole rings is one of the drivers for the (de)localisation of the unpaired electrons towards the C_α and carbonyl O atoms of the **NARID** core this indicates that by altering the aromatic character of the peripheral benzannelated moieties it should also be possible to tune the excited state energies. This could then offer two independent and complementary design handles for the manipulation of excited state energies.

We first consider the size of the peripheral aromatic system by both removing (**BCIBA0**) and adding (**BCIBA2**) linearly fused benzene rings relative to **CIBA**. Looking at the excited state energies it is clear that the addition of linearly fused rings raises both S_1 and T_1 energetically which in the usual context of chromophore design would be considered counterintuitive. Yet, we can rationalise these changes by considering the degree of Hückel-aromaticity in the peripheral rings in the S_0 and T_1 states. In all three cases we observe a gain in aromaticity of the pyrrolic rings when going from S_0 to T_1. In the case of **CIBA** and **BCIBA2** in their S_0 states we observe that the benzene and naphthalene ring systems are aromatic while none of the rings in **BCIBA0** are (Fig. 7, S20 and S21†). Next, also the T_1 state can be understood from the perspective of Clar's sextets as each of the three compounds in this state is described by two Clar's

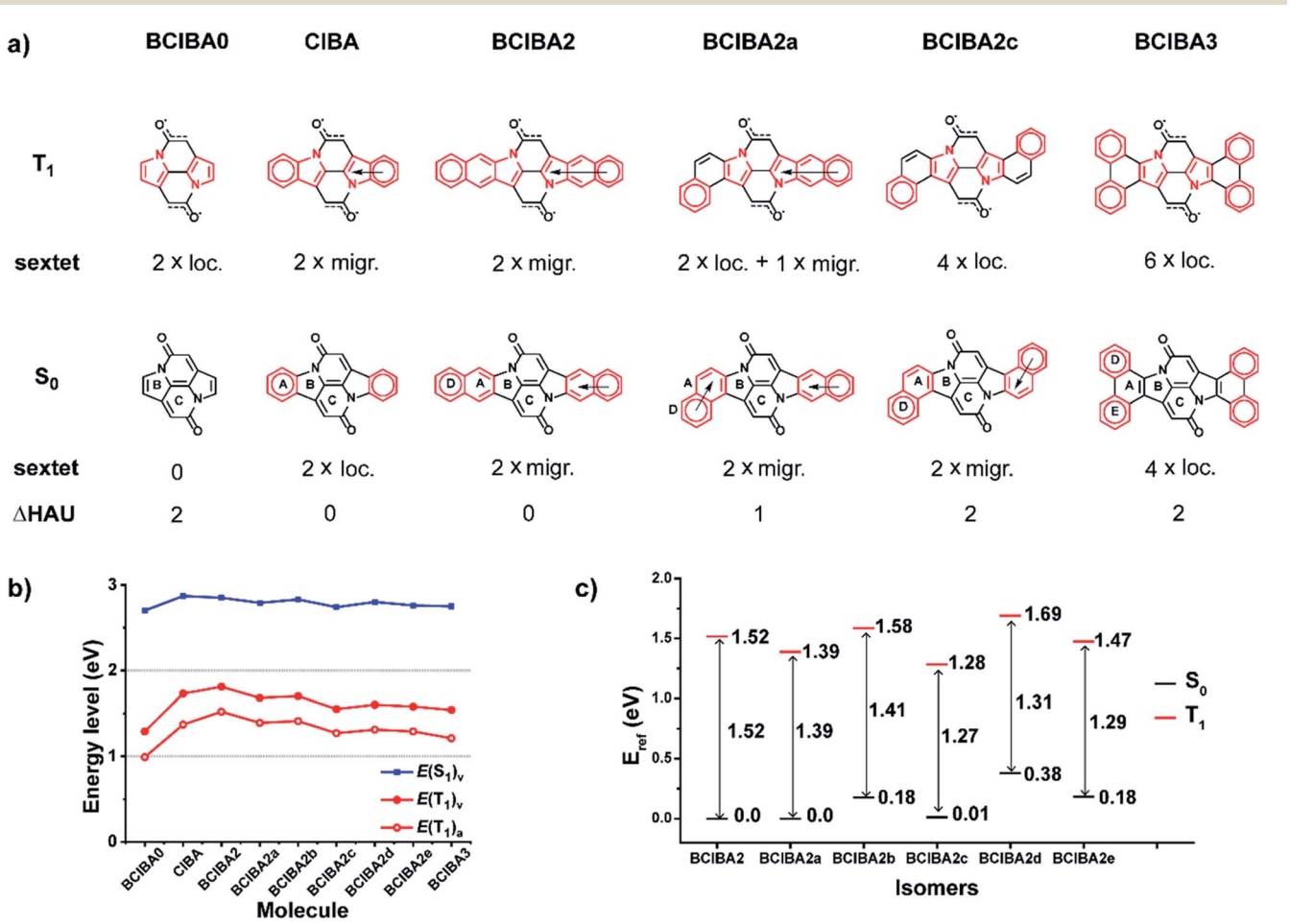

Fig. 7 (a) Chemical structure of **BCIBA**s, the relevant atoms and rings in symmetric positions are signed with an apostrophe. Red units represent cycles which are Clar's sextets in the S_0 and T_1 states, respectively. (b) Plots of excited state energies of the compounds. Subscripted 'v' refers to vertical excitation energies based on S_0 geometries and 'a' refers to adiabatic excitation based on optimized T_1 geometries. (c) Relative energies E_{ref} of the **BCIBA2** isomers in the S_0 and adiabatic T_1 states, with the S_0 state of **BCIBA2** as the reference.

sextets, but in **CIBA** and **BCIBA2** they are migrating while localized in **BCIBA0**. Now, as **BCIBA0** lacks Clar's sextets in its S_0 state while **CIBA** and **BCIBA2** have two each, it becomes obvious that the lower $E(T_1)$ of **BCIBA0** can be rationalized by a relative gain in Hückel-aromaticity upon excitation to T_1. The relative aromaticity gain is smaller for **CIBA** and **BCIBA2** in T_1 as their aromatic units merely expand by incorporating the pyrrole rings. In addition, there is a difference in the S_0 state for the latter two compounds which impacts on $E(T_1)$ as the two migrating sextets of S_0 state **BCIBA2** should provide for an enhanced stability as compared to the two localized sextets of S_0 **CIBA**. Additionally, one can observe more negative NICS values in rings A and D of **BCIBA2** than in ring A of **CIBA** (Fig. 2, S22 and Table S4†).

Next, we considered benzannelated **CIBA** isomers (**BCIBA2a–e**, Fig. 7 and S20†) where each has two migratory Clar's sextets in the S_0 state. There is a variation in the relative energies in the S_0 state, which should be due to steric congestion between the ketone units and the benzene rings. Comparing the $E(T_1)$ of the various **BCIBA2** isomers it is clear that the energies decrease as one goes from a system with low Hückel-aromaticity in the T_1 state such as **BCIBA2** having two migratory sextets, over a system with increased aromaticity, *e.g.*, **BCIBA2a** and **BCIBA2b** with two localized sextets and one migratory, to maximal number of Hückel-aromatic sextets which occurs in the **BCIBA2c** isomer having four localized sextets in their T_1 states. Thus, the connectivity within the benzannelated units allows for tuning of $E(T_1)$ by nearly 0.25 eV (6 kcal mol^{-1}). There are only small variations in the $E(T_1)$ between **BCIBA2a** and **BCIBA2b**, which are equiaromatic,[56] and between the three **BCIBA2c–e** (also equiaromatic), which likely are due to differences in the extent of steric congestion between the benzene and ketone moieties in the T_1 relative to the S_0 state.

Then, when considering the tetrabenzannelated **CIBA** isomers (**BCIBA3** and isomers) we see that the rationale still holds as the isomer with the largest increase in number of Clar's sextets when going from S_0 to T_1 has the lowest $E(T_1)$ (1.26 eV, Fig. S21†). **BCIBA3d**, on the other hand, has the smallest increase in number of Clar's sextets, and accordingly, the largest $E(T_1)$ (1.47 eV). Combined, the calculations demonstrate that through systematic manipulation of the amount of Clar's sextets in the T_1 *vs.* the S_0 state we can qualitatively predict and rationalise trends in the excited state energies.

Five **BCIBA** molecules (including **BCIBA0**) were selected for a detailed analysis on how $E(T_1)$ depends on the delocalization of the unpaired electrons. The $EDDB_H$ plots reveal that the main difference among these molecules occurs at the C atoms of the two pyrrolo units as the delocalization visually varies from one compound to another, while it seems constant at the two C–C=O units (Fig. S23†). There is also a correlation between the amount of delocalization and $E(T_1)$ ($R^2 = 0.98$, Fig. S24†). All in all, we observe that the more delocalized unpaired electrons in the C atoms of the two pyrrolo units, the more stable the T_1 state becomes as the conjugation in this unit increases (Table S3†).

Furthermore, it can be seen that the magnitude of the S_1–T_1 splitting is not constant across the series. For **BCIBA0** we see a relatively large vertical S_1–T_1 splitting of 1.41 eV which diminishes to 1.04 eV in **BCIBA2**. Noteworthy, the HOMO and LUMO are localized similarly in these compounds, but when analysing the electron configurations in the vertically excited S_1 and T_1 states (Table S5†), we find that as the system becomes larger configurations in addition to the singly excited HOMO-to-LUMO excitation become important for the description of the T_1 state. Hence, our assumption on a similarity between the T_1 and S_1 states is not entirely correct, and this is found especially when we move from **BCIBA0** and **CIBA** to **BCIBA2–3**. As the two states are no longer strongly similar in character, we now observe differences in their energy gaps. This highlights that although we can rationalise and tune the excited state energies rather precisely through the understanding and modification of Hückel-aromaticity in the lowest excited states, there remains additional differences between the molecules.

Other modifications of Cibalackrot-type compounds

The **CIBA** scaffold can be viewed as composed of various segments which can be exchanged to other moieties, an

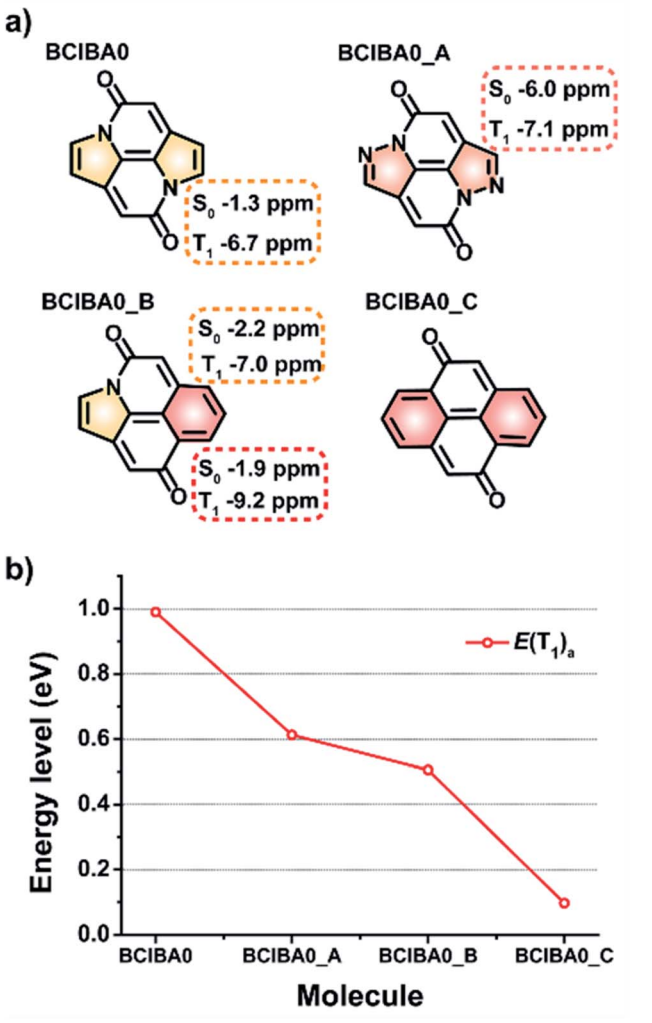

Fig. 8 (a) BCIBA0 and its modified models (BCIBA0_X) with π-$NICS(1.7)_{zz}$ values marked on the modified rings in the S_0 and T_1 states. (b) Plots of adiabatic T_1 excited state energies of the compounds.

apparent first one being a change of the two carbonyl groups to thiocarbonyls, leading to **THIO-CIBA**. This replacement brings down both the $E(T_1)$ and $E(S_1)$ to 0.91 and 2.33 eV, respectively, whereby the $E(S_1)/E(T_1)$ ratio increases compared to the parent **CIBA** from 2.09 to 2.56 (Fig. S24†). Other modifications are replacements of the peripheral benzene rings with heterocycles as well as replacements of the pyrrole rings with rings that either have stronger or weaker Hückel-aromatic character. We specifically probed the replacements of the two pyrrole rings in **BCIBA0** with either pyrazole or benzene rings (Fig. 8). Synthetic routes to non-benzannulated bipyrrolinones and diphenoquinones have been previously shown which would serve as an ideal starting point for the attempted synthesis of these types of compounds.[57–59]

Indeed, with two benzene rings we achieve a modified **BCIBA0** (**BCIBA0_C**) which has a negligible $E(T_1)$ as the attainment of strong Hückel-aromatic character of two benzene rings when the molecule is in T_1 forces the triplet diradical character fully towards the carbonyl O and C_α atoms (Fig. S25†). With one pyrrole and one benzene ring, *i.e.* **BCIBA0_B**, the $E(T_1)$ is intermediate between **BCIBA0** and **BCIBA0_C**. Yet, with two pyrazole rings (**BCIBA0_A**), having weakened Hückel-aromatic character compared to pyrrole,[60] the $E(T_1)$ also moves down, contrary to the simple rationale. Clearly, there are limitations of the approach on modulating the $E(T_1)$ based on the Hückel-aromatic character of the various rings in the **CIBA** and **BCIBA0** scaffolds. The $E(T_1)$ most obviously also depends on bonding features including aromatic character in the S_0 state. This becomes further apparent as one regards imidazole rings in place of the pyrazoles (Fig. S24†).

Combination into a design approach

Having shown that the excited state energies can be tuned by (i) choice of substituents at the C_α atoms, (ii) benzannelations, or (iii) other modifications, we now asked to what extents these approaches can be combined? The **BCIBA3** has a low $E(T_1)$ and the apparent question is to what extent this energy can be

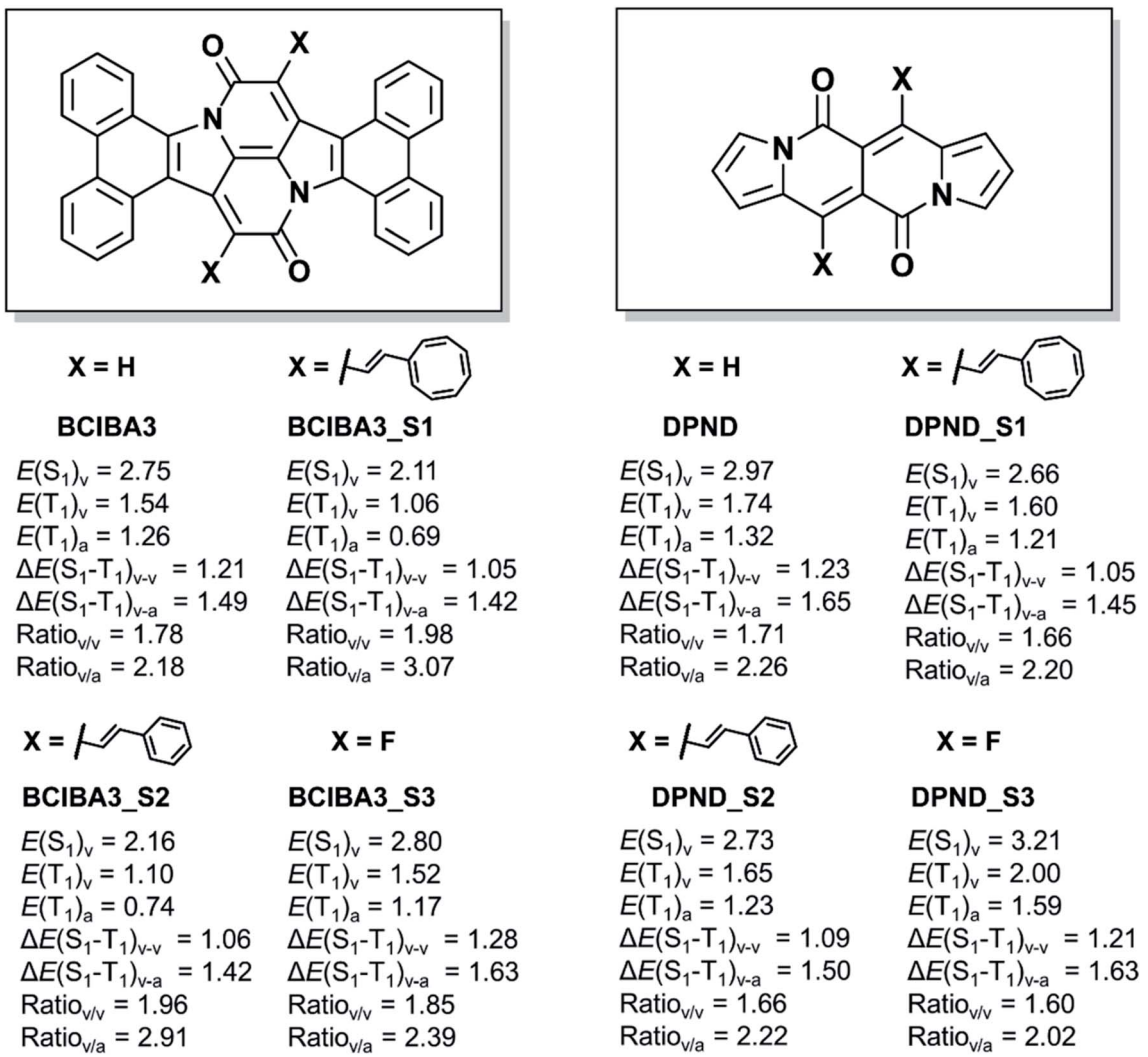

Fig. 9 Chemical structures and relevant excitation energies (in eV) of substituted tetrabenzannelated CIBAs (BCIBA3s) as well as DPNDs. Calculations at TD-M06-2x/def2-SVP//M06-2X/def2-SVP level.

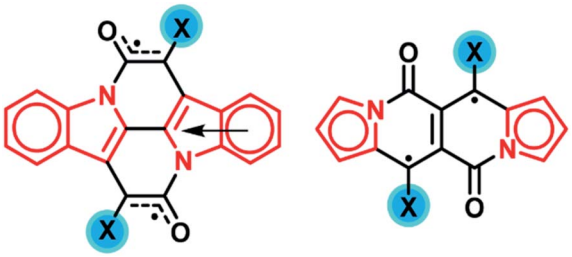

Fig. 10 The main resonance structures of the substituted CIBA and DPND in their T_1 states. The Hückel-aromatic units are marked in red while the substituents X used as handles for tuning $E(T_1)$ are marked in blue.

lowered further by attachment of substituents at the C_α position?

Clearly, with two vinylcyclooctatetraene or two styryl substituents at the C_α atom, one can achieve a lowered $E(T_1)$ and a higher $E(S_1)/E(T_1)$ ratio (**BCIBA3_S1** and **BCIBA3_S2**, Fig. 9), however, a dilemma being that the $E(T_1)$ moves significantly below the ideal value of ~1.1 eV. Instead, to preferentially raise $E(S_1)$ as compared to $E(T_1)$ one may utilize fluoro substitution at C_α, leading to **BCIBA3_S3**. For this compound, the adiabatic $E(T_1)$ is slightly above the 1.1 eV and the $E(S_1)/E(T_1)$ ratios resemble those of **SCIBA1** which functions as a singlet fission chromophore. Using computations, we have thus identified a **CIBA**-based chromophore with high $E(T_1)$ and high $E(S_1)/E(T_1)$ ratio motivating further experimental work towards this or similar compounds.

Importantly, the same approach can be utilized to tailor **DPND**s with targeted excited state energies. By changing the substituents at the site with highest spin density in the T_1 state we can again vary the $E(T_1)$, and also the $E(S_1)/E(T_1)$ ratios as seen in Fig. 9. It is likely that benzannelation also can be utilized to further tune the excited state energies of **DPND**s. Thus, by identifying where the spin density is localized and which units are Hückel-aromatic one can design new singlet fission candidate chromophores.

Conclusions and outlook

Our reanalysis of the Cibalackrot scaffold revealed its Hückel aromatic characters in both the S_0 and T_1 states, instead of Baird-aromatic in the latter. In the triplet state we find that the pyrrolic rings gain Hückel-aromatic character relative to the S_0 state and that the unpaired electrons are delocalized mainly through the central core (**NARID**) of the molecule. By changing the substituents at the site of greatest spin density, *i.e.* at the two C_α atoms, one can effectively adjust the spin density distribution on the chromophore whereby the excited state energy levels can be varied over a wide range (~1 eV). Another means to tune the excited state energies is provided by increasing the Hückel aromatic character in the excited state relative to the ground state by elaborating on the number and type of aromatic sextets of the peripheral aromatic ring system through further benzannelation of the Cibalackrot scaffold.

Taken together, we are able to present a more comprehensive understanding of the nature of the excited states in Cibalackrot-type compounds, their energies and how they can be tuned through tailoring the molecular scaffold whereby novel singlet fission chromophore candidates were identified. Here, it is noteworthy that also dipyrrolonaphthyridinedione (**DPND**) in its T_1 state is Hückel-aromatic instead of Baird-aromatic. This is clear from a similar analysis as provided for the Cibalackrot-type molecules, and it can be rationalized by the structures of Fig. 10. Hence, by choice of substituent at the two C_β atoms, having highest spin density, the $E(T_1)$ of **DPND** can be tuned.

Across the entire field of organic chromophore applications, it is paramount to be able to precisely tune excited states to advance technologies. We argue that without a detailed understanding of these states it is not possible to design new and improved chromophores that can achieve the desired properties. Indeed, tools such as changing substituents at sites of greater/smaller spin density and the manipulation of the excited state aromatic character have hardly been explored within the context of functional organic materials and could provide new and powerful tools to rationally tailor their properties. Earlier, one of us argued that Baird's rule on excited state aromaticity and antiaromaticity can be a handy back-of-an-envelope tool for such design of optically active functional materials.[61] Yet, here we also note the complications, limitations and pitfalls of the excited state aromaticity and antiaromaticity concepts, where Baird-type excited state (anti) aromaticity is the most common form, yet not the only one. Polycyclic systems can be Hückel-aromatic in both the S_0 state and in the lowest excited states, yet with the aromatic character distributed differently between the rings. As Hückel-aromaticity implies a larger number of paired electrons in the aromatic cycle it should, when possible, be preferred over Baird-aromaticity.[41] Hence, care needs to be exercised and one needs to explore what type of aromaticity is at hand in a particular system when in its lowest triplet or singlet excited state. There is otherwise a clear risk of the overuse of the Baird-aromaticity concept to molecules to which it does not apply.

Computational methods

All S_0 and T_1 optimized geometries were obtained using the M06-2X[62] functional together with the def2-SVP basis set.[63] Basing on the optimized ground state geometries, the $E(S_1)$'s were evaluated at TD-DFT M06-2X/def2-SVP level. The $E(T_1)$'s were evaluated with a ΔSCF procedure at DFT M06-2X/def2-SVP level, which manually adjusts the spin multiplicities for both vertical and adiabatic geometries.[64] The electron spin density distributions were analysed with Multiwfn 3.7 (ref. 65) based on the relaxed T_1 state geometries.

Aromaticity was evaluated in terms of the nucleus independent chemical shift (NICS),[43,44] anisotropy of the induced current density (AICD)[45] plots, the aromatic fluctuation index (FLU),[47] and the multicenter index (MCI)[48] computed at the optimized geometries on B3LYP/6-311+G(d,p) level,[66–68] which had been benchmarked and widely used in evaluating aromatic

criteria. NICS values were calculated at 1.7 Å above the ring centers ($NICS(1.7)_{zz}$)[44] using the gauge independent atomic orbital (GIAO)[69] method. The π-only $NICS(1.7)_{zz}$ plots (π-$NICS(1.7)_{zz}$) were obtained by using the sigma-model method implemented in the AROMA package[70] which removes the sigma contributions. NICS-*XY* scans were performed using the AROMA package scanning from 1.7 Å above the plane of the molecule. AICD plots were generated with the AICD 2.0.0 program at 0.050 a.u. isosurface.[45] The harmonic oscillator model of aromaticity (HOMA)[46] measures the geometric aspect of aromaticity and was calculated with Multiwfn 3.7. The FLU and MCI were performed with the ESI-3D collection of programs.[71] Electron delocalization has been also examined using the electron density of delocalization bond ($EDDB_H$)[49,50] at the M06-2X/def2-SVP and B3LYP/6-311+G(d,p) levels. In $EDDB_H$ calculations, Multiwfn and NBO 3.1 (ref. 72) programs have been used, where the latter was employed together with Gaussian 16.[73] $EDDB_H$ surfaces have been visualized using Avogadro.[74,75] Atomic charges and electronic spin densities have been calculated using quantum theory of atoms-in-molecules (QTAIM) scheme,[76] which was done using the "medium quality grid" with a spacing of 0.1 Bohr.

The diradical characters (y_n, $n = 0, 1, 2, \ldots,$) were calculated according to the literature method,[6] with spin-projected UHF (PUHF) theory and 6-311+G(d,p) basis set.

Author contributions

H. O. and O. E. B. formulated the initial idea and developed it together with W. Z., D. W. S. and H. B. Computations were performed by W. Z., O. E. B. and D. W. S. All authors discussed the results, wrote and contributed to the manuscript.

Conflicts of interest

There are no conflicts to declare.

Acknowledgements

W. Z. is grateful to the Marie Skłodowska-Curie grant agreement No. 886066 (EXAM project) for financial support, and W. Z. and H. B. thankfully acknowledge funding by EPSRC (Grants EP/S003126/1). O. E. B. is grateful to the Wenner-Gren Foundations for a postdoctoral fellowship (UPD2018-0305), and D. W. S. acknowledges financial support by the European Union's Framework Programme for Research and innovation Horizon 2020 (2014–2020) under the Marie Skłodowska-Curie Grant Agreement No. 797335 "MulAr-Effect". H. O. gratefully acknowledges financial support from The Swedish Research Council (grant 2019-05618). The computations were enabled by resources provided by the Swedish National Infrastructure for Computing (SNIC) at the National Supercomputer Center (NSC), Linköping, partially funded by the Swedish Research Council through grants 2015-04538 and 2019-05618.

References

1 M. Einzinger, T. Wu, J. F. Kompalla, H. L. Smith, C. F. Perkinson, L. Nienhaus, S. Wieghold, D. N. Congreve, A. Kahn, M. G. Bawendi and M. A. Baldo, *Nature*, 2019, **571**, 90–94.
2 A. Rao and R. H. Friend, *Nat. Rev. Mater.*, 2017, **2**, 17063.
3 J. C. Johnson, A. J. Nozik and J. Michl, *Acc. Chem. Res.*, 2013, **46**, 1290–1299.
4 J. Wen, Z. Havlas and J. Michl, *J. Am. Chem. Soc.*, 2015, **137**, 165–172.
5 T. Ullrich, P. Pinter, J. Messelberger, P. Haines, R. Kaur, M. M. Hansmann, D. Munz and D. M. Guldi, *Angew. Chem., Int. Ed.*, 2020, **59**, 7906–7914.
6 T. Minami and M. Nakano, *J. Phys. Chem. Lett.*, 2012, **3**, 145–150.
7 M. Nakano, *Chem. Rec.*, 2017, **17**, 27–62.
8 O. El Bakouri, J. R. Smith and H. Ottosson, *J. Am. Chem. Soc.*, 2020, **142**, 5602–5617.
9 K. J. Fallon, P. Budden, E. Salvadori, A. M. Ganose, C. N. Savory, L. Eyre, S. Dowland, Q. Ai, S. Goodlett, C. Risko, D. O. Scanlon, C. W. M. Kay, A. Rao, R. H. Friend, A. J. Musser and H. Bronstein, *J. Am. Chem. Soc.*, 2019, **141**, 13867–13876.
10 L. Wang, L. Lin, J. Yang, Y. Wu, H. Wang, J. Zhu, J. Yao and H. Fu, *J. Am. Chem. Soc.*, 2020, **142**, 10235–10239.
11 R. Kotani, L. Liu, P. Kumar, H. Kuramochi, T. Tahara, P. Liu, A. Osuka, P. B. Karadakov and S. Saito, *J. Am. Chem. Soc.*, 2020, **142**, 14985–14992.
12 J. R. Palmer, K. A. Well, J. E. Yarnell, J. M. Favale and F. N. Castellano, *J. Phys. Chem. Lett.*, 2020, **11**, 5092–5099.
13 N. V. Korovina, C. H. Chang and J. C. Johnson, *Nat. Chem.*, 2020, **12**, 391–398.
14 J. Stoycheva, A. Tadjer, M. Garavelli, M. Spassova, A. Nenov and J. Romanova, *J. Phys. Chem. Lett.*, 2020, **11**, 1390–1396.
15 T. Ullrich, D. Munz and D. M. Guldi, *Chem. Soc. Rev.*, 2021, **50**, 3485–3518.
16 B. H. Northrop, K. N. Houk and A. Maliakal, *Photochem. Photobiol. Sci.*, 2008, **7**, 1463–1468.
17 S. S. Zade, N. Zamoshchik, A. R. Reddy, G. Fridman-Marueli, D. Sheberla and M. Bendikov, *J. Am. Chem. Soc.*, 2011, **133**, 10803–10816.
18 E. Hückel, *Z. Phys.*, 1931, **70**, 204–286.
19 H. S. Rzepa, *Chem. Rev.*, 2005, **105**, 3697–3715.
20 Z. S. Yoon, A. Osuka and D. Kim, *Nat. Chem.*, 2009, **1**, 113–122.
21 E. Miliordos, *Phys. Rev. A: At., Mol., Opt. Phys.*, 2010, **82**, 062118.
22 N. C. Baird, *J. Am. Chem. Soc.*, 1972, **94**, 4941–4948.
23 H. Ottosson, *Nat. Chem.*, 2012, **4**, 969–971.
24 M. Rosenberg, C. Dahlstrand, K. Kilså and H. Ottosson, *Chem. Rev.*, 2014, **114**, 5379–5425.
25 R. Papadakis and H. Ottosson, *Chem. Soc. Rev.*, 2015, **44**, 6472–6493.
26 B. Durbeej, J. Wang and B. Oruganti, *ChemPlusChem*, 2018, **83**, 958–967.

27 J. Oh, Y. M. Sung, Y. Hong and D. Kim, *Acc. Chem. Res.*, 2018, **51**, 1349–1358.
28 C. Liu, Y. Ni, X. Lu, G. Li and J. Wu, *Acc. Chem. Res.*, 2019, **52**, 2309–2321.
29 G. Markert, E. Paenurk and R. Gershoni-Poranne, *Chem.–Eur. J.*, 2021, DOI: 10.1002/chem.202005248.
30 M. Bühl and A. Hirsch, *Chem. Rev.*, 2001, **101**, 1153–1184.
31 A. Hirsch, Z. Chen and H. Jiao, *Angew. Chem., Int. Ed.*, 2000, **39**, 3915–3917.
32 D. Shukla and P. Wan, *J. Am. Chem. Soc.*, 1993, **115**, 2990–2991.
33 P. Wan and E. Krogh, *J. Chem. Soc., Chem. Commun.*, 1985, 1207–1208.
34 F. Feixas, J. Vandenbussche, P. Bultinck, E. Matito and M. Solà, *Phys. Chem. Chem. Phys.*, 2011, **13**, 20690–20703.
35 P. B. Karadakov, *J. Phys. Chem. A*, 2008, **112**, 7303–7309.
36 P. B. Karadakov, *J. Phys. Chem. A*, 2008, **112**, 12707–12713.
37 M. Rosenberg, H. Ottosson and K. Kilså, *Phys. Chem. Chem. Phys.*, 2011, **13**, 12912–12919.
38 Y. M. Sung, M.-C. Yoon, J. M. Lim, H. Rath, K. Naoda, A. Osuka and D. Kim, *Nat. Chem.*, 2015, **7**, 418–422.
39 L. A. Paquette, M. J. Broadhurst, P. Warner, G. A. Olah and G. Liang, *J. Am. Chem. Soc.*, 1973, **95**, 3386–3387.
40 K. Jorner, F. Feixas, R. Ayub, R. Lindh, M. Solà and H. Ottosson, *Chem.–Eur. J.*, 2016, **22**, 2793–2800.
41 S. Escayola, C. Tonnelé, E. Matito, A. Poater, H. Ottosson, M. Solà and D. Casanova, *Angew. Chem., Int. Ed.*, 2021, DOI: 10.1002/anie.202100261.
42 B. Oruganti, J. Wang and B. Durbeej, *Org. Lett.*, 2017, **19**, 4818–4821.
43 A. Stanger, *J. Org. Chem.*, 2006, **71**, 883–893.
44 R. Gershoni-Poranne and A. Stanger, *Chem.–Eur. J.*, 2014, **20**, 5673–5688.
45 D. Geuenich, K. Hess, F. Köhler and R. Herges, *Chem. Rev.*, 2005, **105**, 3758–3772.
46 T. M. Krygowski, *J. Chem. Inf. Comput. Sci.*, 1993, **33**, 70–78.
47 E. Matito, M. Duran and M. Solà, *J. Chem. Phys.*, 2005, **122**, 014109.
48 P. Bultinck, R. Ponec and S. V. Damme, *J. Phys. Org. Chem.*, 2005, **18**, 706–718.
49 D. W. Szczepanik, M. Andrzejak, K. Dyduch, E. Żak, M. Makowski, G. Mazur and J. Mrozek, *Phys. Chem. Chem. Phys.*, 2014, **16**, 20514–20523.
50 D. W. Szczepanik, M. Andrzejak, J. Dominikowska, B. Pawełek, T. M. Krygowski, H. Szatylowicz and M. Solà, *Phys. Chem. Chem. Phys.*, 2017, **19**, 28970–28981.
51 M. Swart, *Theor. Chem. Acc.*, 2020, **139**, 160.
52 Y. Wu, Y. Wang, J. Chen, G. Zhang, J. Yao, D. Zhang and H. Fu, *Angew. Chem., Int. Ed.*, 2017, **56**, 9400–9404.
53 J. L. Ryerson, A. Zaykov, L. E. A. Suarez, R. W. A. Havenith, B. R. Stepp, P. I. Dron, J. Kaleta, A. Akdag, S. J. Teat, T. F. Magnera, J. R. Miller, Z. Havlas, R. Broer, S. Faraji, J. Michl and J. C. Johnson, *J. Chem. Phys.*, 2019, **151**, 184903.
54 Z. T. Armstrong, M. B. Kunz, A. C. Jones and M. T. Zanni, *J. Phys. Chem. C*, 2020, **124**, 15123–15131.
55 A. Zaykov, P. Felkel, E. A. Buchanan, M. Jovanovic, R. W. A. Havenith, R. K. Kathir, R. Broer, Z. Havlas and J. Michl, *J. Am. Chem. Soc.*, 2019, **141**, 17729–17743.
56 P. W. Fowler, S. Cotton, D. Jenkinson, W. Myrvold and W. H. Bird, *Chem. Phys. Lett.*, 2014, **597**, 30–35.
57 H.-D. Becker and K. Gustafsson, *Tetrahedron Lett.*, 1976, **17**, 4883–4886.
58 K. Hemming, A. D. Redhouse, R. K. Smalley, J. R. Thompson, P. D. Kennewell and R. Westwood, *Tetrahedron Lett.*, 1992, **33**, 2231–2234.
59 G. Pfeiffer and H. Bauer, *Liebigs Ann. Chem.*, 1980, 564–576.
60 S. Dey, D. Manogaran, S. Manogaran and H. F. Schaefer, *J. Phys. Chem. A*, 2018, **122**, 6953–6960.
61 H. Möllerstedt, M. C. Piqueras, R. Crespo and H. Ottosson, *J. Am. Chem. Soc.*, 2004, **126**, 13938–13939.
62 Y. Zhao and D. G. Truhlar, *Theor. Chem. Acc.*, 2008, **120**, 215.
63 J. Zheng, X. Xu and D. G. Truhlar, *Theor. Chem. Acc.*, 2011, **128**, 295.
64 D. Padula, Ö. H. Omar, T. Nematiaram and A. Troisi, *Energy Environ. Sci.*, 2019, **12**, 2412–2416.
65 T. Lu and F. Chen, *J. Comput. Chem.*, 2012, **33**, 580–592.
66 A. D. Becke, *J. Chem. Phys.*, 1993, **98**, 5648–5652.
67 P. J. Stephens, F. J. Devlin, C. F. Chabalowski and M. J. Frisch, *J. Chem. Phys.*, 1994, **98**, 11623–11627.
68 R. Krishnan, J. S. Binkley, R. Seeger and J. A. Pople, *J. Chem. Phys.*, 1980, **72**, 650–654.
69 K. Wolinski, J. F. Hinton and P. Pulay, *J. Am. Chem. Soc.*, 1990, **112**, 8251–8260.
70 A. Stanger and A. Rahalkar, *AROMA*, http://schulich.technion.ac.il/Amnon_Stanger.htm.
71 E. Matito, *ESI-3D: Electron Sharing Indexes Program for 3D Molecular Space Partitioning*, Institute of Computational Chemistry, Girona, 2006, http://iqc.udg.edu/~eduard/esi.
72 E. D. Glendening, A. E. Reed, J. E. Carpenter and F. Weinhold, *NBO 3.1*.
73 M. J. Frisch, G. W. Trucks, H. B. Schlegel, G. E. Scuseria, M. A. Robb, J. R. Cheeseman, G. Scalmani, V. Barone, G. A. Petersson, H. Nakatsuji, *et al.*, *Gaussian 16, Revision B.01*, Gaussian, Inc., Wallingford CT, 2016.
74 *Avogadro: an open-source molecular builder and visualization tool. Version 1.2.0*.
75 M. D. Hanwell, D. E. Curtis, D. C. Lonie, T. Vandermeerschd, E. Zurek and G. R. Hutchison, *J. Cheminf.*, 2012, **4**, 17.
76 R. F. W. Bader, *Chem. Rev.*, 1991, **91**, 893–928.